Comparison of Elastic and Elastic-Plastic Structural Analyses for Cooled Turbine Blade Airfoils

Albert Kaufman

JULY 1980

NASA

NASA Technical Paper 1679

Comparison of Elastic and Elastic-Plastic Structural Analyses for Cooled Turbine Blade Airfoils

Albert Kaufman
Lewis Research Center
Cleveland, Ohio

Summary

Von Mises effective stress and total and plastic strain states in cooled turbine blade airfoils were calculated for the initial takeoff transient of an advanced technology engine (1990 time frame) with a blade relative effective gas temperature of 1400° C and a gas inlet total pressure of 2860 kilopascals at maximum takeoff. Three analytical approaches were considered: a three-dimensional elastic-plastic analysis using the MARC nonlinear finite-element structural computer code, a three-dimensional elastic analysis using MARC with the identical finite-element model, and a one-dimensional elastic-plastic beam-theory analysis. Eight cases involving different combinations of thermal and mechanical loads and two cooling configurations were analyzed. One of the cooling configurations was an all-impingement cooled system in which air flowed through holes in an internal sheet metal insert to impinge on the inner surface of the airfoil shell. The second cooling configuration also utilized impingement cooling with the addition of angled leading-edge film-cooling holes.

The results at maximum takeoff showed agreement in terms of effective total strains between the MARC elastic-plastic and elastic analyses within 9 percent for rotating airfoils and 28 percent for stationary airfoils with the elastic results on the conservative side. Poor agreement was shown between stress distributions computed from the three-dimensional finite-element and one-dimensional beam-theory elastic-plastic analyses, particularly at the hot gas side airfoil surfaces.

Introduction

The trend toward increased turbine blade tip speeds and gas temperatures in advanced aircraft engines has resulted in turbine blade airfoil stresses at critical locations that exceed the yield strength of the material. The computation of stress-strain states in a complex geometry such as a cooled turbine blade undergoing plastic flow is a formidable problem requiring the use of nonlinear finite-element codes such as MARC (ref. 1). These nonlinear codes are not currently used as blade design tools because of the extensive demands they make on computer resources. Nonlinear structural analyses also require cyclic material properties and transient metal temperatures which are frequently too unreliable to justify the cost of this type of analysis.

Current practice in turbine blade structural design is to use simplified analytical methods and approximations as design tools. One approach which has found widespread use is to calculate the total strains at the maximum load condition of the engine cycle from an elastic finite-element analysis and to apply these as total strain ranges for cyclic life calculations. This method is based on the assumption that the total strain in a structure undergoing plastic flow can be predicted from an elastic stress analysis. Although the calculated stresses from an elastic analysis will be incorrect, more accurate stresses and the plastic strains can be estimated from the total strains and the known stress-strain behavior of the material. A further refinement of this approach is the method of elastic strain invariance (ref. 2) wherein the total strain ranges are calculated from elastic analyses of both the maximum and minimum load conditions.

Another common approach in turbine blade design has been the use of one-dimensional elastic-plastic analyses based on the beam theory assumption that plane sections remain plane (ref. 3). The relative simplicity and rapid solution time of beam theory computer programs in comparison to finite-element programs makes them attractive for turbine blade design. However, the beam theory approach is of questionable validity for airfoils with small aspect ratios and nonlinear spanwise temperature gradients (ref. 4).

The purpose of this study was to compare stress and strain states derived from elastic finite-element and elastic-plastic beam-theory methods to results from an elastic-plastic finite-element analysis for the complex geometries and thermo-mechanical loading conditions of cooled turbine blade airfoils. This is one of a series of studies of cooled gas turbine blades; the results of previous studies are reported in references 5 and 6.

Three-dimensional elastic and elastic-plastic finite-element analyses of cooled turbine blade airfoils were performed for an initial engine takeoff transient using the MARC nonlinear structural analysis computer program. The analyses were based on the takeoff conditions of an advanced technology

aircraft engine with a blade relative effective gas temperature of 1400° C and a gas inlet total pressure of 2860 kilopascals at maximum takeoff. The eight cases studied involved different combinations of thermal and mechanical loads for each of two impingement cooling configurations—one with and one without leading-edge film-cooling holes. One-dimensional beam-theory analyses were also performed for some cases. Comparisons were made of the von Mises effective stress-strain states at maximum takeoff computed from the simpler analytical approaches to the results of the elastic-plastic finite-element analyses. Creep effects were not considered in this study.

Analytical Procedure

Stress-strain states in cooled turbine blade airfoils were calculated for an assumed takeoff transient of an advanced technology aircraft engine.

Conditions of Analyses

The analyses were based on the estimated operating conditions during takeoff of a first-stage turbine blade in an advanced high-bypass-ratio turbofan engine being studied for use in commercial passenger aircraft in the 1990's.

Figure 1 illustrates the airfoil cooling system. Air flows radially up the cavity formed by an internal sheet metal insert and then flows through an array of holes in the insert to impingement cool the inside surface of the airfoil shell. Two versions of this cooling system were considered: an all-impingement-cooled configuration and a similar impingement-cooled configuration with the addition of a row of leading-edge film-cooling holes.

A 5-second takeoff transient was assumed from a midspan blade relative effective gas temperature of 670° C at idle to 1400° C at maximum takeoff. The gas inlet total pressure was 2860 kilopascals and the coolant to gas flow ratio was 0.117 at maximum takeoff.

Eight analytical cases were studied (table I). The cases designated with R were for rotating airfoils and those designated with S were for stationary airfoils. Cases designated with an I involved all-impingement-cooled airfoils, while those with an F involved impingement-cooled airfoils with leading-edge film-cooling holes. In cases RIH and RFH, the centrifugal loading included the mass of the impingement insert. In cases RI and RF, only the centrifugal loading of the airfoil shell was considered. Cases RIH, RI, and SI had identical thermal loading, as did cases RFH, RF, and SF. The metal temperatures for cases SIH

TABLE I. – ANALYTICAL CASES

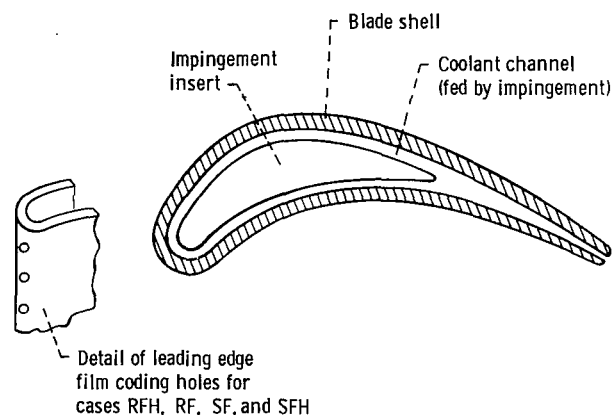| Case	Airfoil cooling configurations	Centrifugal loading	Thermal loading
RIH	All impingement	Airfoil, impingement insert	Figure 2(a)
RFH	Impingement, leading edge film cooled	Airfoil, impingement insert	Figure 2(b)
RI	All impingement	Airfoil	Figure 2(a)
RF	Impingement, leading edge film cooled	Airfoil	Figure 2(b)
SI	All impingement	None	Figure 2(a)
SF	Impingement, leading edge film cooled		Figure 2(b)
SIH	All impingement		Figure 2(a) +28° C
SFH	Impingement, leading edge film cooled		Figure 2(b) +28° C

Figure 1. – Airfoil cooling configurations.

and SFH were increased 28° C over the comparable metal temperatures for cases SI and SF, respectively; this was done to simulate the higher temperatures that a stator vane would be exposed to, compared to a rotor blade for the same turbine stage. Hence, the designation H for the rotating cases signifies higher centrifugal load while for the stationary cases, H signifies higher temperatures.

Input for Analyses

The airfoil geometry, transient temperatures, and mechanical loads which were used as input to the structural analysis computer programs were based on the turbine blade design and operating conditions of the candidate aircraft gas turbine engine.

Geometry.—The blade airfoil had a span length of 3.8 centimeters, an aspect ratio of 1, a wall thickness taper from 0.13 centimeter at the hub to 0.08 centimeter at the tip (outside surface contour constant from hub to tip), and a hub to tip radius ratio of 0.85. The holes in the leading-edge film-cooled configuration were 0.05 centimeter in diameter with a spacing of 10 diameters and were angled 30° to the surface in the spanwise direction. A cross section of the airfoil is shown in figure 1.

Material properties.—The assumed blade material was cast in 100 alloy. Stress-strain properties for this alloy were obtained from reference 7, and the mean coefficient of thermal expansion data (subsequently converted to instantaneous values) was obtained from reference 8. These data were entered into MARC as functions of temperature. The program linearly interpolates from these data for the local temperature at any airfoil location. The material properties used in the analyses are presented in table II.

Thermomechanical loading.—Transient metal temperatures were calculated from the TACT1 thermal analysis computer program (ref. 9). TACT1 was developed at the NASA Lewis Research Center to compute time-dependent three-dimensional temperature distributions in turbine blade airfoils cooled by impingement and crossflow convection. Coolant side heat-transfer coefficients were calculated in the program using published correlations. Local film cooling is also handled in the program using an effectiveness correlation based on converting the geometry of the film-cooling holes to that of equivalent slots. Local temperature gradients around cooling holes were not accounted for in the heat-transfer analysis.

Computed airfoil leading-edge stagnation point and trailing-edge temperatures at midspan are shown in figure 2 for the takeoff transient between idle and maximum takeoff. The temperature response of figure 2(a) applied to the all-impingement-cooled

TABLE II. – PROPERTIES OF IN 100 MATERIAL USED IN ANALYSES

(a) Stress-strain[a] properties (ref. 7)

Temperature, °C	Modulus of elasticity, GPa	Strength, MPa			Reduction in area, percent
		Ultimate	0.02-Percent yield	0.2-Percent yield	
21	226	989	610	763	14
850	158	766	605	727	8
925	156	567	347	461	12
1000	129	387	198	294	20

[a]Poisson's ratio, 0.3; density, 7750 kg/m^3.

(b) Mean coefficient of thermal expansion (21° C to temperature)10^{-6}/°C (ref. 8)

Temperature, °C	Coefficient	Temperature, °C	Coefficient
93	13.0	649	14.4
204	13.0	760	14.9
316	13.1	871	15.8
427	13.5	982	16.7
538	13.9	1093	18.2

airfoil cases RIH, RI, and SI, while the temperature response of figure 2(b) applied to the leading-edge film-cooled airfoil cases RFH, RF, and SF. Airfoil temperature transients for cases SIH and SFH were 28° C higher than those shown in figures 2(a) and (b), respectively.

A temperature rise of approximately 190° C per second occurred during the steepest part of the transient between 1 and 2 seconds of lapsed time. The airfoil temperature rise leveled off after 3 seconds into the takeoff transient. At maximum takeoff when the highest gas pressure during the flight would occur, the maximum temperature difference between the inside and outside walls located at the leading-edge stagnation point was about 190° C. This temperature gradient across the leading-edge wall resulted in tensile thermal stresses at the inside surface which were additive to the centrifugal stresses. The leading-edge temperature in the film-cooled airfoil (fig. 2(b)) was 70° C less than in the all-impingement-cooled airfoil (fig. 2(a)).

Temperature contour plots at maximum takeoff are presented at the airfoil outside pressure and suction surfaces viewed from inside the wall in figure 3
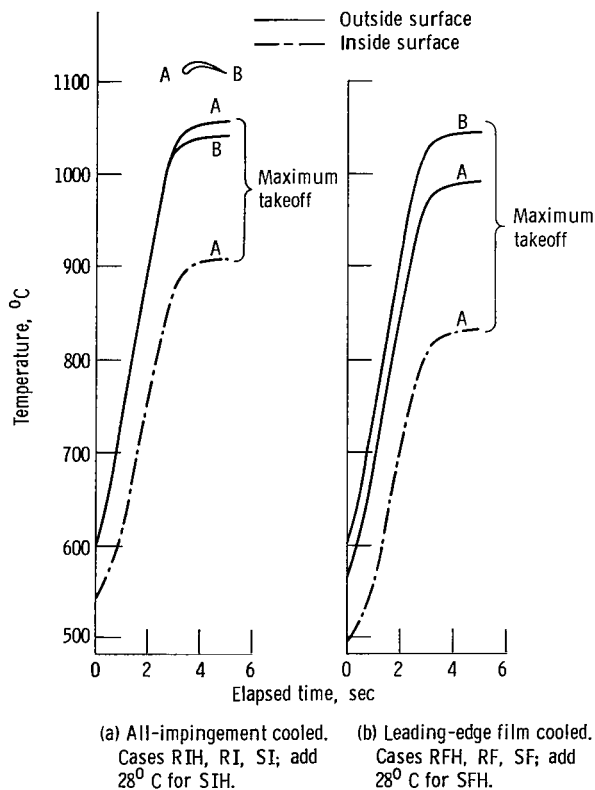
for cases RIH, RI, and SI and in figure 4 for cases RFI, RF, and SF. The maximum metal temperatures of 1040° C for the all-impingement-configuration of figure 3 and 1030° C for the film-cooled configuration of figure 4 are somewhat lower than the maximum temperatures shown in figure 2 of approximately 1060° C for both configurations, because the contours of figures 3 and 4 actually apply to Gaussian integration points slightly inside the wall. Both cooling configurations had leading-edge spanwise temperature gradients of about 150° C. Similar
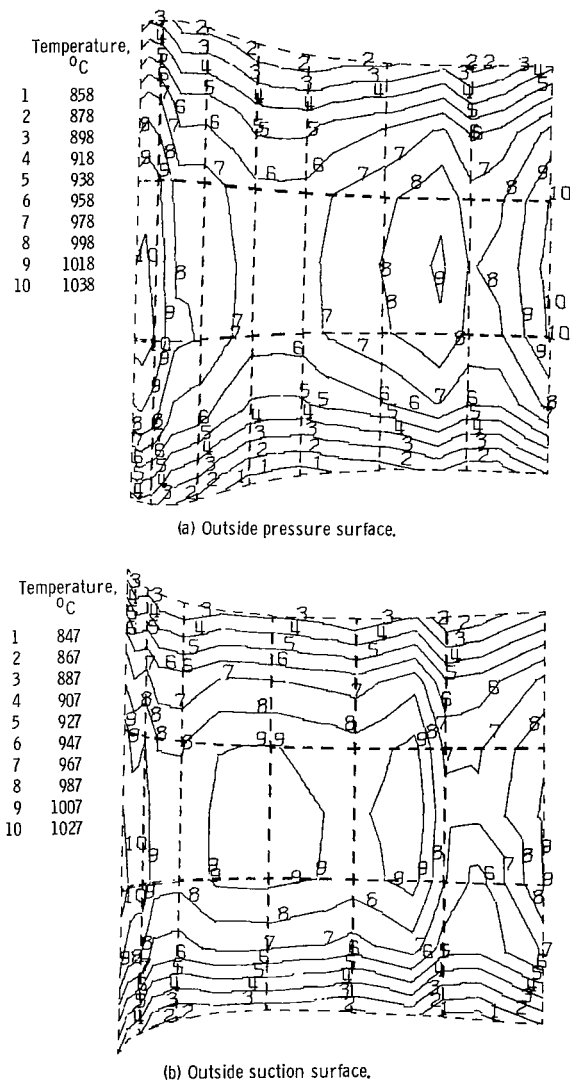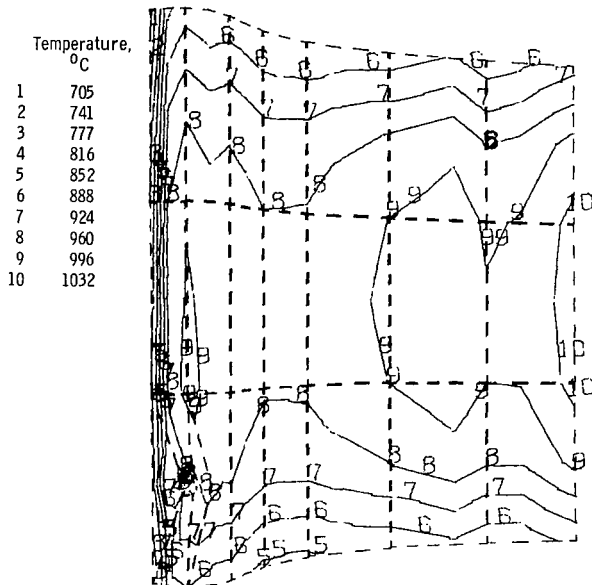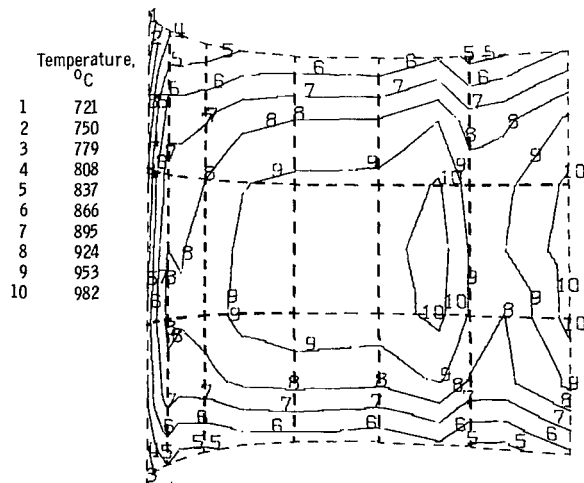

	Temperature, °C
1	858
2	878
3	898
4	918
5	938
6	958
7	978
8	998
9	1018
10	1038

(a) Outside pressure surface.

	Temperature, °C
1	847
2	867
3	887
4	907
5	927
6	947
7	967
8	987
9	1007
10	1027

(b) Outside suction surface.

Figure 3. - Metal temperature distribution at maximum takeoff for all-impingement-cooled airfoil for cases RIH, RI, and SI; add 28° C for case SIH.

——— Outside surface
— — — Inside surface

(a) All-impingement cooled. Cases RIH, RI, SI; add 28° C for SIH.

(b) Leading-edge film cooled. Cases RFH, RF, SF; add 28° C for SFH.

Figure 2. - Airfoil metal temperature - time response (midspan).

temperature distributions for cases SIH and SFH would be obtained by adding 28° C to all the values in the temperature code tables in figures 3 and 4, respectively.

Centrifugal and gas pressure load effects were incorporated into MARC for cases RI and RF in the form of increments of rotative speed and gas pressure for each transient load increment. For cases RIH and RFH, the centrifugal loading due to the mass of the
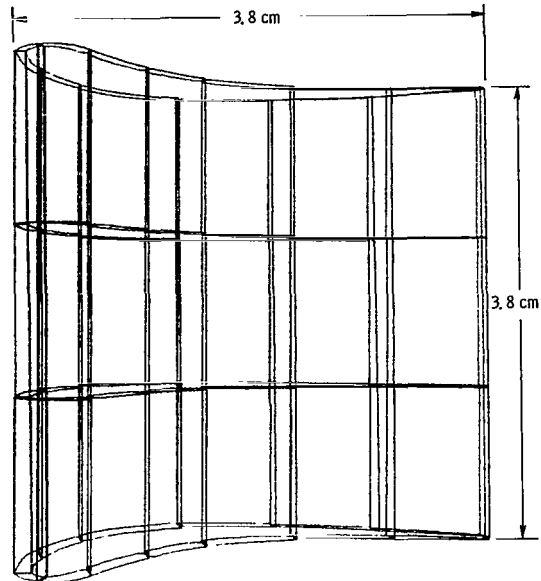

	Temperature, °C
1	705
2	741
3	777
4	816
5	852
6	888
7	924
8	960
9	996
10	1032

(a) Outside pressure surface.

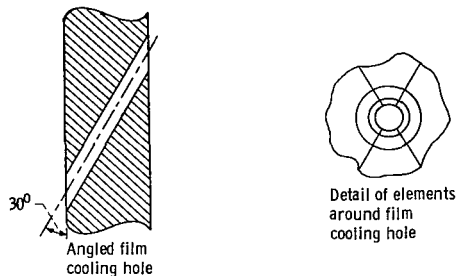|	Temperature, °C
1	721
2	750
3	779
4	808
5	837
6	866
7	895
8	924
9	953
10	982

(b) Outside suction surface.

Figure 4. – Metal temperature distribution at maximum takeoff for leading-edge film-cooled airfoil for cases RFH, RF, and SF; add 28° C for case SFH.

(a) All-impingement-cooled airfoil (cases RIH, RI, SI, and SIH).

30°

Angled film cooling hole

Detail of elements around film cooling hole

(b) Leading-edge film-cooled airfoil (cases RFH, RF, SF, and SFH).

Figure 5. – Finite-element models.

insert was applied to the airfoil shell as uniform distributed loading along the span. At maximum takeoff, the average centrifugal stress at the airfoil hub was 170 megapascals for cases RI and RF and 233 megapascals for cases RIH and RFH.

Methods of Analysis

Airfoil stress-strain distributions and histories during the takeoff transients were computed from the MARC nonlinear, finite-element structural analysis computer program (ref. 1). Plasticity computations were performed over a series of time increments during the engine transient. Plastic strain behavior is based on incremental plasticity theory using the von Mises yield criterion and a normality flow rule. Centrifugal and gas pressure loads and local metal temperatures determined from TACT1 were input into MARC for each of 27 Gaussian integration points in each element of the finite-element model. Both elastic and elastic-plastic analyses were performed with the identical finite-element model using MARC. The material yield strength was set to a fictitiously high level for the elastic analyses. The elastic analyses were compared to the elastic-plastic analyses for the same time increment in which the latter exhibited the highest plastic strains. Although temperature, stress, and strain contour plots are presented for the outer and inner aircoil surfaces, these results are obtained from computation at integration points inside the wall (about 11 percent of the local wall thickness).

Elastic-plastic stress-strain analyses were also performed using a one-dimensional stress program based on the beam theory assumption that plane sections remain plane (ref. 3). The beam theory analyses used the same thermal and mechanical load transients and material properties as were used in the MARC analyses. The area of the airfoil cross section under consideration in the beam theory analysis was divided into elements of area with centroid locations which approximately coincided with the Gaussian integration points in the finite-element model at the comparable span location.

Finite-Element Analysis

Finite-element models are illustrated in figure 5(a) for the all-impingement-cooled airfoil and in figure 5(b) for the leading-edge film-cooled airfoil. These configurations were modeled with 20 node, isoparametric three-dimensional elements. Only one cooling hole was modeled for the film-cooled airfoil because of limitations on computer storage and execution time. The all-impingement-cooled airfoil model (fig. 5(a)) had 39 elements with 349 nodes and

977 unsuppressed degrees of freedom, while the film-cooled airfoil (fig. 5(b)) had 46 elements with 405 nodes and 1145 unsuppressed degrees of freedom.

The effects of the blade platform and dovetail attachment were simulated by fixing the airfoil hub plane against motion in the spanwise direction. Rigid body motion was prevented by constraining one hub leading-edge node in all directions and a hub trailing-edge node in the circumferential direction.

An exaggerated stress concentration effect results from only modeling a single hole, since the presence of adjacent holes tends to reduce the peak stresses at the hole rim. In order to compensate for this conservative approach, the leading-edge film-cooling hole in the finite-element model of figure 5(b) was placed at the slightly less critical one-sixth span height from the airfoil hub rather than at the 30-percent span height which would be expected to be the most critical location. The one-sixth span position was also a more convenient location for modeling an angled hole.

The accuracies of the analyses were checked as much as possible by verifying the centrifugal stress distributions without thermal loading for the all-impingement-cooled airfoil (cases RIH and RI). A check of the accuracy of the finite-element model for the film-cooled airfoil was obtained by analyzing an airfoil with a hole axis normal to the surface and with no thermal loading. An elastic stress concentration factor of 2.85 was obtained for an integration point 0.003 centimeter from the hole rim; this compares to a theoretical stress concentration factor of 3.0 at the rim of a central hole in a uniaxially loaded plate.

Each takeoff transient was divided into 17 increments of temperature and mechanical load. Both the elastic and elastoplastic analyses over this load spectrum with MARC required approximately 10 hours of computing time on the Univac 1100. In contrast, an elastic-plastic analysis with the beam-type computer program required a matter of minutes. An elastic-plastic analysis with MARC, which was performed on a CDC 7600 computer, used only approximately 1000 seconds of computer time.

Results and Discussion

Stress-strain distributions were calculated for cooled turbine blade airfoils during the takeoff transient of an advanced technology commercial aircraft engine. Eight cases involving different combinations of thermal and mechanical loading and two cooling configurations were studied. Stress-strain states were calculated by both elastic and elastic-plastic finite-element analyses and also by a one-dimensional elastic-plastic beam theory analysis.

TABLE III. – FINITE-ELEMENT ANALYSIS EFFECTIVE STRAIN RESULTS AT LOCATIONS

OF HIGHEST PLASTIC STRAINS

Case	Three-dimensional elastic–plastic analysis					Three-dimensional elastic analysis	
	Effective, total strain, ϵ_T, microstrain	Effective plastic strain, ϵ_P, microstrain	Percent off σ–ϵ curve	Corrected ϵ_T, microstrain	Corrected ϵ_P, microstrain	ϵ_T, microstrain	Calculated ϵ_P, microstrain
RIH	1690	100	5.7	1590	120	1650	140
	1380	90	9.2	1270	130	1300	140
	1060	90	2.7	1030	130	1030	130
RFH	4100	520	1.4	4050	560	4020	540
	2690	480	.5	2700	520	2570	410
	2620	400	.3	2620	450	2460	330
RI	2410	220	6.9	2260	290	2300	320
	2060	180	3.1	2000	200	1940	190
	2100	160	1.8	2060	170	1990	150
RF	2730	550	0.4	2740	610	2550	460
	2780	510	1.6	2740	610	2520	430
	3970	490	.1	3970	490	3900	440
SI	1500	330	2.0	1470	460	1380	380
	1370	250	5.1	1300	220	1260	210
	1490	220	5.6	1410	240	1340	100
SF	4910	2170	3.8	4740	2220	4160	1760
	3750	780	10.6	3390	1140	3260	1030
	3480	740	8.5	3210	990	2940	770
SIH	1660	540	9.0	1530	550	1350	410
	1630	450	9.2	1490	690	1390	400
	1760	420	16.4	1510	500	1450	450
SFH	5250	2800	10.0	5830	3450	4220	2140
	3200	1260	1.2	3240	1080	2950	1040
	3990	1180	12.2	3560	1600	3300	1390

Three-Dimensional Elastic-Plastic Finite-Element Analyses

The results of the three-dimensional, elastic-plastic analyses using MARC are presented in table III. These results are given in terms of effective total and plastic strains for the three highest plastic strain locations shown in the computer printouts for each of the eight cases studied. In order to restrict the amount of computer paper generated, a prior judgement had to be made as to the parts of the airfoil which were of most interest and the expected most critical locations in the airfoils. In some cases, computer contour plots later exhibited somewhat higher plastic strains at Gaussian integration points which were omitted for printout purposes. However, the differences in strains between the actual locations of highest plastic strain and those in the computer
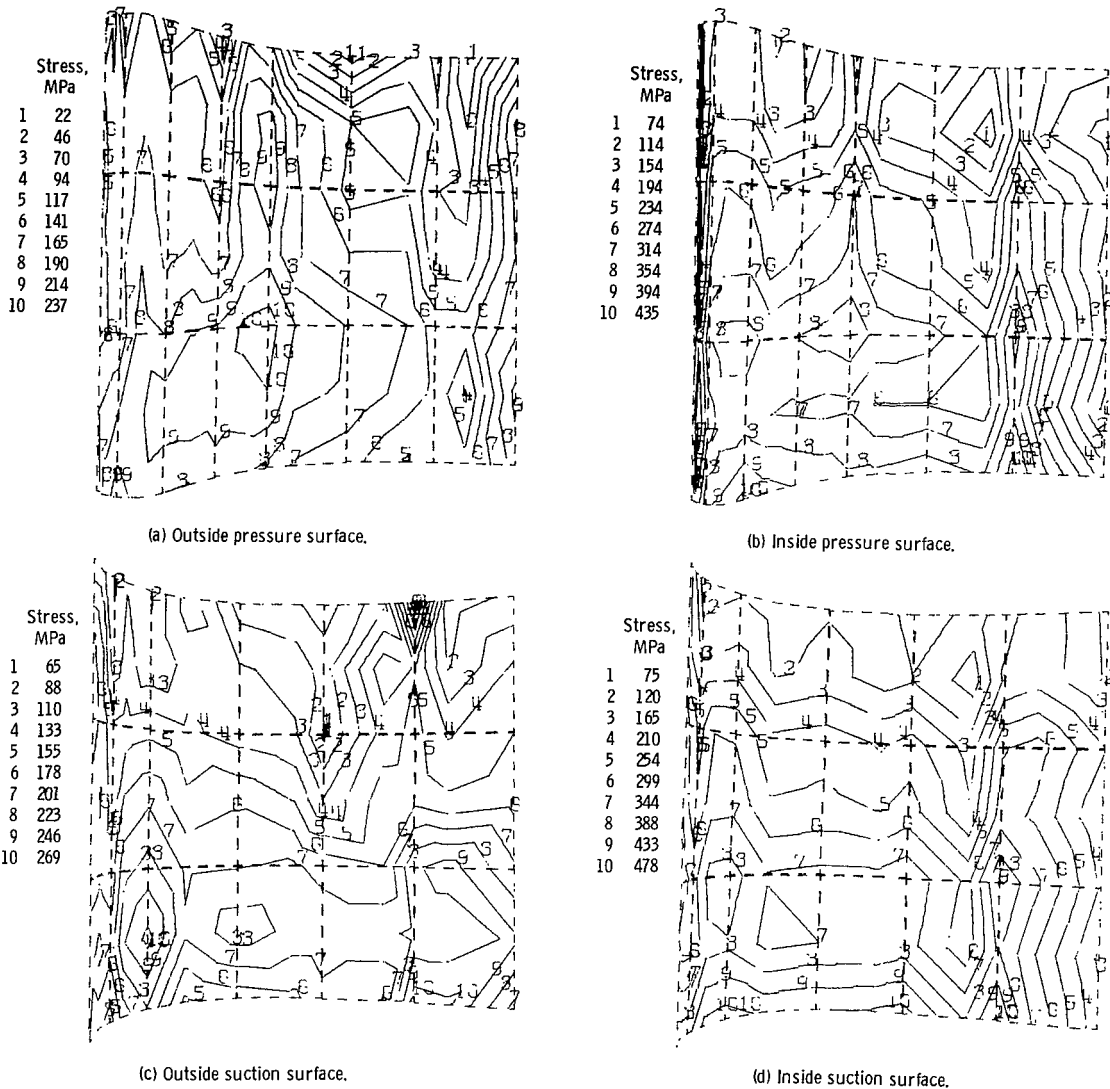
Stress, MPa	
1	22
2	46
3	70
4	94
5	117
6	141
7	165
8	190
9	214
10	237

(a) Outside pressure surface.

Stress, MPa	
1	74
2	114
3	154
4	194
5	234
6	274
7	314
8	354
9	394
10	435

(b) Inside pressure surface.

Stress, MPa	
1	65
2	88
3	110
4	133
5	155
6	178
7	201
8	223
9	246
10	269

(c) Outside suction surface.

Stress, MPa	
1	75
2	120
3	165
4	210
5	254
6	299
7	344
8	388
9	433
10	478

(d) Inside suction surface.

Figure 6. – Effective stress distribution at maximum takeoff for case RIH.

printout were not significant and did not affect the validity of this study. The highest plastic strains were at maximum takeoff with some exceptions in cases RFH, RF, and SFH which occurred between 2 and 4 seconds of elapsed time during the takeoff transient.

The first two columns under "Three-dimensional elastic-plastic analysis" in table III give the computed effective total and plastic strains from the MARC analyses. A measure of the accuracy of the solution is how well the stress-strain values lie on the input material stress-strain curves; a significant discrepancy usually indicates that the temperature differences between load increments were too large for the iteration algorithm to handle. The percent discrepancy between the computed effective total strains and the material stress-strain relations is also given in table III. These discrepancies were generally under 10 percent, although there was an instance in case SIH where it was as much as 16 percent. The effective total and plastic strains were corrected to lie on the stress-strain curves at approximately half the offset in both stress and total strain. The corrected

8

effective total and plastic strains are given in table III in the next two columns after the "percent off σ-ϵ curve" column. The highest total and plastic strains were calculated for the stationary film-cooled airfoils. Typical effective stress and plastic strain contours are shown in figures 6 and 7 for the inner and outer airfoil surfaces for case RIH. The largest plastic strain is shown at the outside suction surface in figure 7(b) near the leading edge and is slightly higher than the maximum computed plastic strain for

case RIH shown in table III. The plastic strains on the airfoil inner surface were negligible and, therefore, plastic strain contours are not shown in figure 7 for the inner surface. In general, the largest plastic strains occurred in the all-impingement-cooled airfoil at the outer surface near the leading edge and in the film-cooled airfoil at the rim of the film-cooling hole on the inside surface of the airfoil.

Elastic Finite-Element Analysis Evaluation

The effective total strains computed from the MARC three-dimensional elastic analyses are also presented in table III for each of the three high plastic strain locations for each of the eight cases for the same elapsed times at which the highest plastic strains were reached during the elastic-plastic analyses. Effective total strains from the elastic analyses are compared to the computed and corrected effective total strains from the elastic-plastic analyses in figures 8(a) and (b), respectively. If perfect agreement existed, the 24 plotted points (eight cases with three highest plastic strain locations) would all fall along the 45° line. Both the computed and corrected effective total strains from the elastic-plastic analysis were generally larger than those from the elastic analysis (figs. 8(a) and (b)). An improved correlation between the elastic and elastic-plastic results was obtained when the latter were corrected to lie on the stress-strain curves (fig. 8(b)). The agreement between the effective total strains from the elastic and elastic-plastic MARC analyses was reasonably good for values less than 4000 microstrain. The worst discrepancies between the elastic and elastic-plastic results were 9 percent for the rotating airfoils and 28 percent for the stationary airfoils with the elastic results being comparatively conservative.

If the effective total strains computed from the elastic analyses are assumed to be correct, the corresponding effective stresses and plastic strains can be obtained from the known stress-strain relations of the material. Calculated effective plastic strains derived in this manner from the elastic analyses are presented in the last column of table III. Correlations of effective plastic strains determined from elastic and elastic-plastic MARC analyses are shown in figures 8(c) and (d). Again, a somewhat better correlation was obtained with the corrected elastic-plastic results except at the largest strain values (fig. 8(d)). Generally, the plastic strains predicted from the elastic analyses were smaller than the corrected plastic strains based on the elastic-plastic analyses. The largest plastic strains occurred at the leading-edge holes in the stationary film-cooled airfoil cases. The worst discrepancies between the
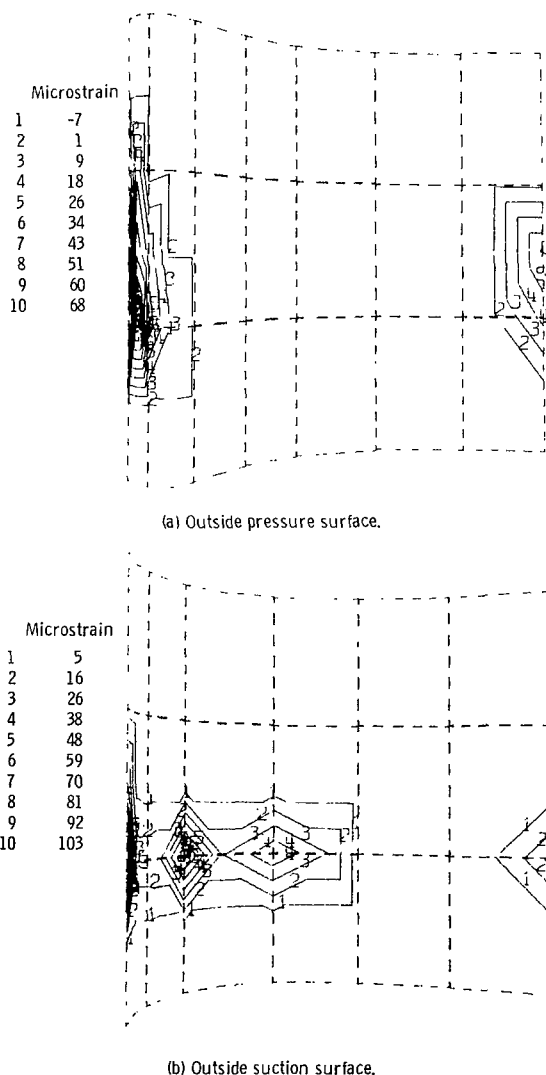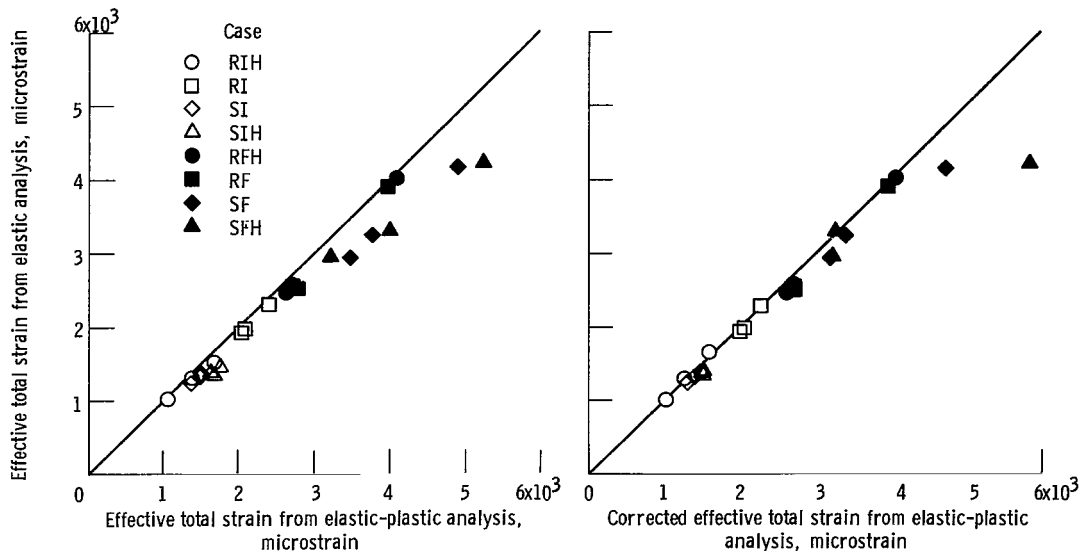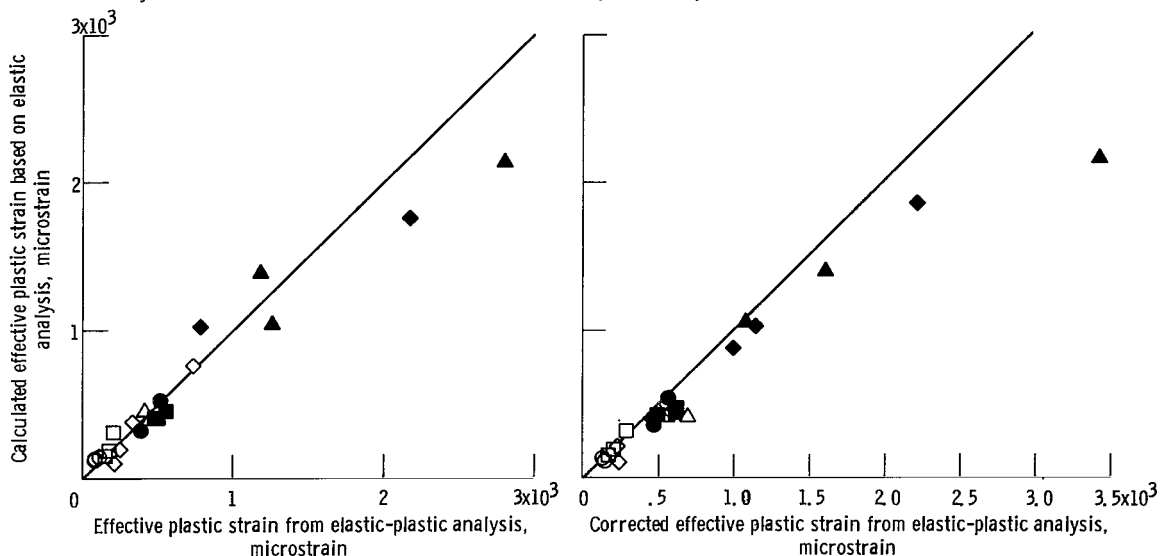

(a) Outside pressure surface.

	Microstrain
1	-7
2	1
3	9
4	18
5	26
6	34
7	43
8	51
9	60
10	68

	Microstrain
1	5
2	16
3	26
4	38
5	48
6	59
7	70
8	81
9	92
10	103

(b) Outside suction surface.

Figure 7. - Effective plastic strain distribution at maximum takeoff for case RIH.

Figure 8. – Comparison of elastic with elastic-plastic finite-element stress analysis results. (Refer to table I for case conditions.)

plastic strains derived from the elastic and elastic-plastic analyses were 30 percent for rotating airfoils and 40 percent for stationary airfoils with the predictions from the elastic results again on the conservative side.

A possible reason for the better agreement between elastic and elastic-plastic strain computations for rotating airfoils is that the centrifugal load tends to reduce the maximum effective total strain levels, as

compared to stationary airfoils, because it counteracts the maximum thermal strains which are compressive.

Beam Theory Evaluation

A one-dimensional analysis based on beam theory was performed for each of the four cases involving the all-impingement-cooled airfoil configuration at
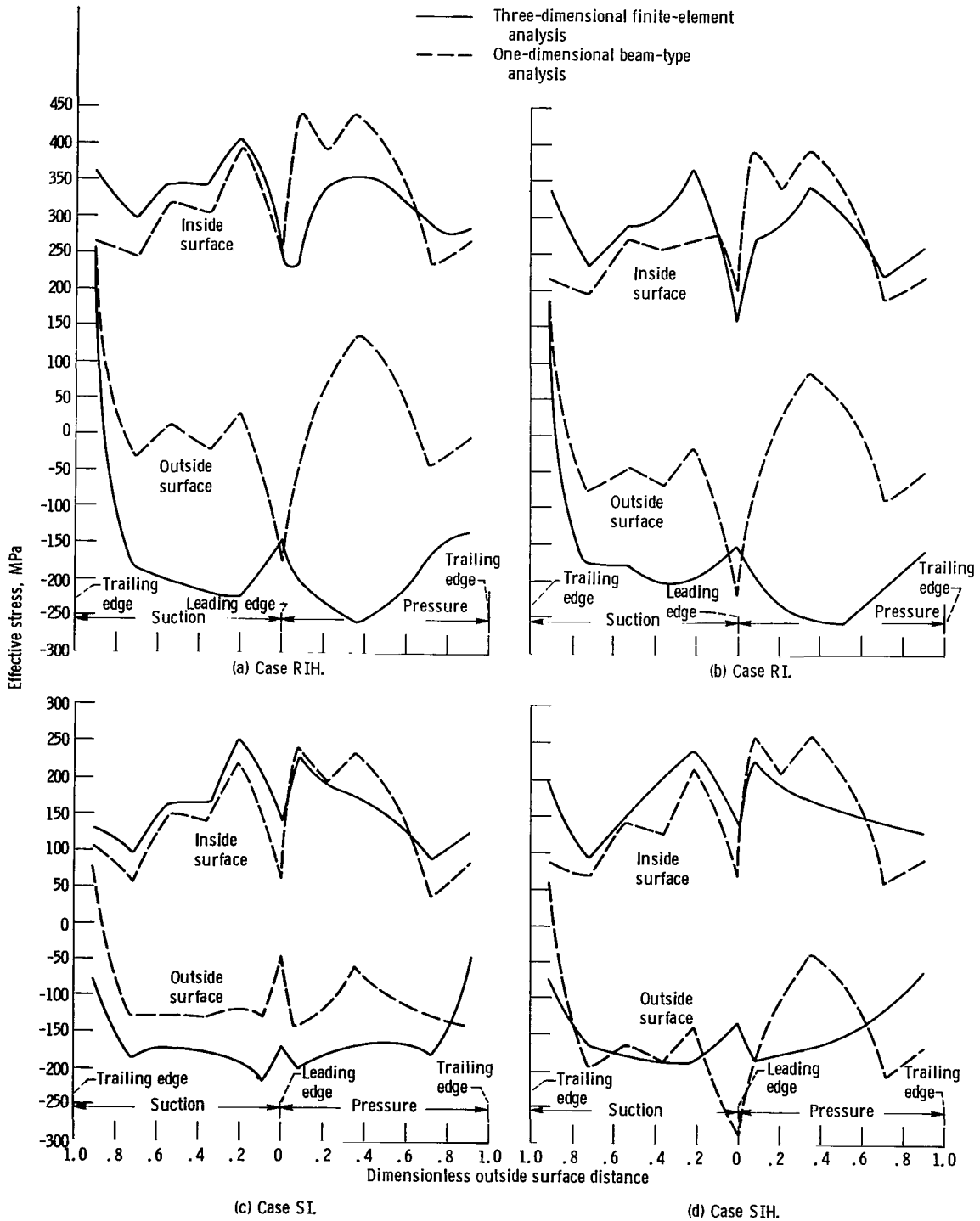
Figure 9. - Comparison of stress distributions from one- and three-dimensional analyses of all-impingement-cooled airfoils (30-percent span).

the critical 30-percent span height location. Since the beam-theory approach does not directly account for stress concentrations such as cooling holes, the film-cooled cases were not considered for purposes of analysis evaluation. Stress distributions around the airfoil inside and outside surfaces are shown in figure 9 for the all-impingement-cooled cases.

For comparison, effective stress distributions at the airfoil surfaces from the MARC elastic-plastic analyses are also shown in figure 9. Signs were assigned to the effective stresses using the guidelines given in reference 10 for determining the dominant stress direction from the signs and magnitudes of the principal stresses.

Better agreement between the one- and three-dimensional elastic-plastic analyses was obtained for the cooler inner surface of the airfoil than for the hot-gas-side outer surface where the bulk of the plastic flow occurred. Better agreement is also seen for the stationary airfoil cases SI and SIH (figs. 9(c) and (d)). One of the major reasons for the discrepancies between the one- and three-dimensional results is that, for the latter, the high thermal stresses result in considerable variations in the maximum principal stress directions. The one-dimensional stresses are always normal to the plane of the airfoil span section under consideration. In terms of effective total and plastic strains, the agreement between the MARC and beam theory analyses was so poor that detailed comparisons were not worthwhile. As an example, although the MARC elastic-plastic analyses predicted plastic strains in cases RIH and RI, the beam theory analyses indicated no plastic strains for these cases.

Summary of Results

The major results of this study of analytical methods for calculating the von Mises effective elastic-plastic stress and strain states at the end of the engine takeoff transient in impingement-cooled turbine blade airfoils with and without leading-edge film cooling were as follows:

1. The effective total strains calculated from the elastic finite-element analysis were in reasonably good agreement with the effective total strains from the elastic-plastic finite-element analyses except when the total strains were above 4000 microstrain. Effective total and plastic strains derived from the elastic analyses were generally smaller than the elastic-plastic results.

2. The worst discrepancies in effective total strains calculated from the elastic finite-element analyses, as compared to those calculated from the elastic-plastic finite-element analysis, were 9 percent for rotating airfoils and 28 percent for stationary airfoils with the elastic results on the conservative side.

3. The worst discrepancies in effective plastic strains derived from the elastic finite-element analysis and the material stress-strain relations, as compared to those calculated from the elastic-plastic finite-element analysis, were 30 percent for rotating airfoils and 40 percent for stationary airfoils with the elastic results on the conservative side.

4. The one-dimensional stresses calculated from elastic-plastic beam-theory analyses gave poor agreement with the elastic-plastic finite-element results, particularly at the hot-gas-side airfoil surfaces. Agreement between the one- and three-dimensional analyses was worse for rotating airfoils than for stationary airfoils.

Lewis Research Center,
    National Aeronautics and Space Administration,
        Cleveland, Ohio, January 22, 1980,
            505-01.

References

1. MARC General Purpose Finite Analysis Program. User Manual Vol. A and B, MARC Analysis Research Corporation, 1979.

2. Manson, S.S.: Thermal Stress and Low-Cycle Fatigue. McGraw-Hill Book Co., Inc., 1966.

3. Stewart, W.L.; and Vogel, W.H.: Methods for Predicting Thermal Stress Cracking in Turbine Stator or Rotor Blades. (PWA-3142, Pratt and Whitney Aircraft; NASA Contract NAS3-7909.) NASA CR-54636, 1967.

4. Boley, B.A.; and Weiner, J.H.: Theory of Thermal Stresses. John Wiley & Sons, Inc., 1960, pp. 307-355.

5. Kaufman, A.; and Gaugler, R.E.: Thermal-Structural Mission Analyses of Air-Cooled Gas Turbine Blades. NASA TM-78963, 1978.

6. Kaufman, A.; and Gaugler, R.E.: Cyclic Structural Analyses of Air-Cooled Gas Turbine Blades and Vanes. NASA TM X-73494, 1976.

7. Fritz, L.J.; and Koster, W.P.: Tensile and Creep Rupture Properties of (16) Uncoated and (2) Coated Engineering Alloys at Elevated Temperatures. (REPT-931-21300, Metcut Research Associates, Inc.; NASA Contract NAS3-18911.) NASA CR-135138, 1977.

8. High Temperature High Strength Nickel Base Alloys. Second ed. International Nickel Company of Canada, Ltd., 1968.

9. Gaugler, R.E.: TACT1, A Computer Program for the Transient Thermal Analysis of a Cooled Turbine Blade or Vane Equipped with a Coolant Insert. I—Users Manual. NASA TP-1271, 1978.

10. Manson, S.S.; and Halford, G.R.: Treatment of Multiaxial Creep-Fatigue by Strainrange Partitioning. NASA TM X-73488, 1976.

1. Report No. NASA TP-1679	2. Government Accession No.	3. Recipient's Catalog No.
4. Title and Subtitle COMPARISON OF ELASTIC AND ELASTIC-PLASTIC STRUCTURAL ANALYSES FOR COOLED TURBINE BLADE AIRFOILS		5. Report Date July 1980
		6. Performing Organization Code
7. Author(s) Albert Kaufman		8. Performing Organization Report No. E-241
9. Performing Organization Name and Address National Aeronautics and Space Administration Lewis Research Center Cleveland, Ohio 44135		10. Work Unit No. 505-01
		11. Contract or Grant No.
12. Sponsoring Agency Name and Address National Aeronautics and Space Administration Washington, D.C. 20546		13. Type of Report and Period Covered Technical Paper
		14. Sponsoring Agency Code

15. Supplementary Notes

16. Abstract

Elastic-plastic stress-strain states in cooled turbine blade airfoils were calculated by three methods for the initial takeoff transient of an advanced technology aircraft engine. The three analytical methods compared were a three-dimensional elastic-plastic finite-element analysis, a three-dimensional elastic finite-element analysis, and a one-dimensional elastic-plastic beam-theory analysis. Structural analyses were performed for eight cases involving different combinations of mechanical and thermal loading on impingement cooled airfoils with and without leading-edge film-cooling holes. The von Mises effective total strains at maximum takeoff computed from the elastic and elastic-plastic finite-element analyses agreed within 9 percent for rotating airfoils and 28 percent for stationary airfoils with the elastic results on the conservative side.

17. Key Words (Suggested by Author(s)) Turbine blades Structures	18. Distribution Statement Unclassified – unlimited STAR Category 39

19. Security Classif. (of this report) Unclassified	20. Security Classif. (of this page) Unclassified	21. No. of Pages 14	22. Price* A02

SPECIAL FOURTH CLASS MAIL
BOOK

U.S.MAIL

```
3    1 1U,D,        070380 S00903DS
DEPT OF THE AIR FORCE
AF WEAPONS LABORATORY
ATTN: TECHNICAL LIBRARY (SUL)
KIRTLAND AFB NM 87117
```

NASA